NUCET NUCLEAR ENERGY AND TECHNOLOGY

Nuclear Energy and Technology 10(3): 199–204
DOI 10.3897/nucet.10.137455

Research Article

Modelling of oxide fuel restructuring during first hours after a reactor reaches its power*

Vladimir I. Folomeev[1], Svetlana M. Ganina[1], Natalya E. Astakhova[1]

1 *IPPE JSC, 1 Bondarenko Sq., 249033 Obninsk, Kaluga Reg., Russia*

Corresponding author: Svetlana M. Ganina (smgan@ippe.ru)

Academic editor: Georgy Tikhomirov ♦ **Received** 3 April 2024 ♦ **Accepted** 17 September 2024 ♦ **Published** 8 October 2024

Citation: Folomeev VI, Ganina SM, Astakhova NE (2024) Modelling of oxide fuel restructuring during first hours after a reactor reaches its power. Nuclear Energy and Technology 10(3): 199–204. https://doi.org/10.3897/nucet.10.137455

Abstract

There is a substantial amount of experimental data that confirm the peculiarity of the oxide fuel behavior during the first hours after a reactor reaches its power. With an increase in temperature during the said period, oxide fuel pellets crack because of a significant temperature gradient. Further developments occur due to the accumulation and redistribution of fission products, and manifest themselves as changes in the fuel matrix porosity and the formation (or diameter increase) of a central hole. The zones that differ in their microstructure, density and thermal conductivity are formed along the fuel pellet radius. As the oxide fuel composition and restructuring result in its thermal conductivity change, it is important to pay attention to the formulas used in the stress-strain state calculations of a fuel element. The methodology for calculating changes in the oxide fuel porosity and the pellet's internal diameter is proposed and based on the published research papers dedicated to the study of oxide fuel properties and behavior during the first hours after a reactor reaches its power. The methodology was tested using real experimental data on the porosity redistribution along the fuel pellet radius. The presence and the size of the pellet's inner hole, as well as changes in the fuel matrix porosity, have a noticeable effect on the maximum temperature value. Taking into account the pellet structure evolution while performing computational simulation of the fuel rod operation under irradiation allows assessing the fuel element's operability more accurately. The proposed methodology can be used in computer codes designed to calculate the stress-strain state of cylindrical fuel elements of fast reactors.

Keywords

oxide fuel, porosity, restructuring, fuel pin, fuel pellet, experimental data, stress-strain states (SSS)

Introduction

There is an array of experimental data that confirm the specific behavior of oxide fuel in the initial hours after the reactor rise to power. As the reactor rises initially to power and temperature grows, the oxide fuel pellets crack because of a major temperature gradient. Fuel pieces move filling partially the gap between fuel and the cladding and leading so to crack formation.

After the reactor rises to power and operating temperatures are reached, there is a fuel mass transfer taking place in the fuel pellets in the direction that is opposite to the temperature gradient as a result of porosity migration and thermally activated evaporation and condensation processes, and bulk and surface diffusion. These processes lead to the crack healing, the formation of a central hole in fuel (or an increase in its diameter if there is a hole in the initial state), and a noticeable decrease in the gap between

* Russian text published: Russian text published: Izvestiya vuzov. Yadernaya Energetika (ISSN 0204-3327), 2024, n. 2, pp. 202–212.

Copyright *Folomeev VI et al.* This is an open access article distributed under the terms of the Creative Commons Attribution License (CC-BY 4.0), which permits unrestricted use, distribution, and reproduction in any medium, provided the original author and source are credited.

fuel and the cladding (depending on the linear power value and, accordingly, the fuel temperature, there is a potential for the fuel-cladding gap elimination). Zones are formed that differ in the fuel microstructure, density and thermal conductivity.

In the process of porosity migration, column-shaped grains are formed that have a radial orientation, the grains grow rapidly, and equiaxial grains are formed when the temperature is in excess of a certain value. On the colder peripheral part (outer radius) of the fuel pellet, fuel remains non-restructured (Degaltsev et al. 1987; Freund 1990). An approximate temperature range corresponding to the three-zone structure boundaries is given in Olander 1976; Kozlov et al. 2004; Kinev 2011. The effect of burnup and operating temperature on the fuel microstructure and the dimensions of the pellet inner radius is analyzed as new data are obtained from post-irradiation examinations (Venkiteswaran et al. 2014; Parrish et al. 2020; Cappia et al. 2023). The oxide fuel restructuring also leads to a change in thermal conductivity, therefore, much attention is paid to determining more accurately the dependences that describe the thermal conductivity of fresh and irradiated oxide fuel (Magni et al. 2020; Bonev et al. 2023).

Based on the literature overview, a fairly simple methodology was chosen to calculate the change in porosity and the fuel column central hole diameter. The following assumptions are used:

- all pores have the same size, and their volume does not depend on the radial position and time; no collisions between migrating pores and their coalescence are taken into account;
- pores are closed and migrate in the radial direction only.

Pore conservation equation

Pore conservation equation (Olander 1976):

$$\frac{dp}{dt} = \frac{1}{r}\frac{\partial}{\partial r}\left[r \cdot V_p \cdot p\right] \tag{1}$$

Initial and boundary conditions:

$$\begin{aligned} P(r,0) &= p_0, \\ P(\infty,t) &= p_0 \end{aligned} \tag{2}$$

where p is the current porosity value, p_0 is the initial porosity, V_p is the pore displacement rate, r is the radius, and t is the time.

To obtain the numerical solution, we shall break down the radius into Nf calculation cells (intervals). We shall integrate equation (1) for the interval $[r_{i-1/2}, r_{i+1/2}]$ ($i = 0, Nf$). As the result of the transformations, we will have the following equation:

$$p_{i-1/2} = \frac{Vp_{i+1/2} \cdot r_{i+1/2} \cdot p_{i+1/2} - \dfrac{p_{i+1/2}}{2 \cdot (t_j - t_{j-1})} \cdot \dfrac{r_{i+1/2}^2 - r_{i-1/2}^2}{2} + \dfrac{\widetilde{p}_i}{(t_j - t_{j-1})} \cdot \dfrac{r_{i+1/2}^2 - r_{i-1/2}^2}{2}}{\dfrac{1}{2 \cdot (t_j - t_{j-1})} \cdot \dfrac{r_{i+1/2}^2 - r_{i-1/2}^2}{2} + Vp_{i-1/2} \cdot r_{i-1/2}} \tag{3}$$

where $p_i = \dfrac{p_{i+1/2} + p_{i-1/2}}{2}$, and $\widetilde{p}_i$ is the porosity value in the center of the interval $[r_{i-1/2}, r_{i+1/2}]$ at the previous time point.

Since $P(\infty,t) = p_0$, we may search for the value of the porosity on the calculation cell boundaries beginning from the fuel outer boundary.

Pore displacement rate

The pore displacement rate is deteremined by equation (Olander 1976):

$$V_p = \left(\frac{A \cdot \Omega}{R \cdot T}\right) \cdot Dg \cdot \left(\frac{\Delta H_{vap}}{R \cdot T}\right) \cdot \exp\left(\frac{\Delta S_{vap}}{R}\right) \exp\left(-\frac{\Delta H_{vap}}{R \cdot T}\right) \left(\frac{1}{T}\frac{dT}{dr}\right), \tag{4}$$

where V_p is the pore rate in mm/s; A is the constant ($A = 3.3914 \cdot 10^{19}$); R is the gas constant ($R = 8.314$ J/(mole·K)); Ω is the fuel molecule volume ($\Omega = A^3$ for UO_2), the formula uses value $\Omega = 41 \cdot 10^{-21}$ mm^3; and D_g is the coefficient of the fuel molecule diffusion in gas that can be written as:

$$D_g = D_g^* \cdot \left(\frac{T}{2000}\right)^{3/2} \cdot \left(\frac{1}{P_g}\right) \tag{5}$$

where $D_g^* = 1100$ mm^2/s (for He); T is the temperature, K; and P_g is the total gas pressure in the pore, atm:

$$P_g = T / T_{sint}; \tag{6}$$

$T_{sint} = 1800$–1900 K is the fuel pellet sintering temperature; and ΔH_{vap}, (J/mole); ΔS_{vap}, (J/(mole·K) is the solid body evaporation heat and entropy.

The following dependence option is presented in Lackey et al. 1972 for the pore displacement rate calculation:

$$V_p = -\frac{Material_const \cdot P_0 \cdot e^{-\Delta H_{vap}/RT}}{P_g \cdot T_K^{3/2}} \cdot \frac{dT}{dr} \cdot 3600. \tag{7}$$

$$\begin{aligned} \mathrm{Ln}(P_0 \cdot e^{-\Delta H/RT}) = {} & -212.275 + 65.842 \cdot O/M + \\ & 8.9453 \cdot 10^{-02} \cdot T_K - 2.55399 \cdot 10^{-02} \cdot \\ & O/M \cdot T_K + 2.9560 \cdot O/M^2 - 5.6541 \cdot 10^{-06} \cdot T_K^2, \end{aligned} \tag{8}$$

where V_p is the pore rate, in mm/s; $Material_const$ is the material constant = 3.364; P_0 is the material constant; ΔH_{vap} is the evaporation heat; O/M is the stoichiometry; R is the gas constant; T_K is the temperature, K; P_g is the total gas pressure in the pore, atm (it is assumed in the calculation that $P_g = T / T_{sint}$); and dT/dr is the temperature gradient, K/mm.

To calculate displacement rates, the paper uses an additional parameter, $Param$ ($Param = 0.1$), which allows one to record the pore displacement rates in region Δ (with a minor temperature gradient) on the internal hole boundary side. The pellet inner radius is

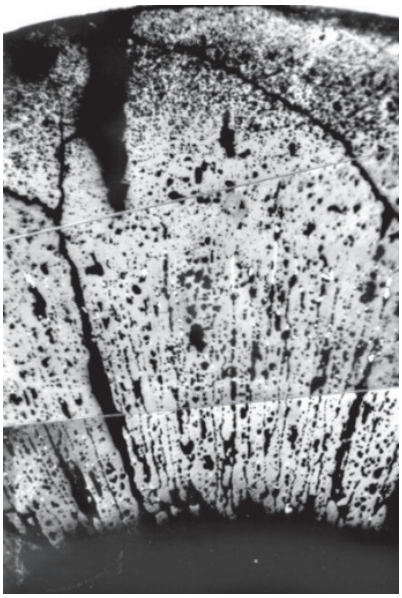

Figure 1. MOX fuel structure with a burnup of 9.4% h.a. in the BN-600 reactor (×50) (Kozlov et al. 2004).

not actually a smooth surface with uniform porosity (Fig. 1), and due to the introduction of value Δ, the pore displacement rate in this area is determined as a certain average value.

With the calculated radius value being $r_i < r_0 + \Delta$, we assume that the pore displacement rate is $Vp_i = Vp_{i+1}$.

Here, $\Delta = (r_{Nf} - r_0) \cdot Param$; r_i is the value of the radius on the calculation cell boundary at the given time point ($i = 0, Nf$); and r_0 is the value of the fuel pellet inner radius at the given time point.

Calculation of the mesh boundary position change along the fuel radius

We shall write the equation for each cross-section along the radius with reliance on the mass conservation equation:

$$(\tilde{r}^2_{i+1/2} - \tilde{r}^2_{i-1/2}) \cdot (1 - \tilde{p}_i) = (r^2_{i+1/2} - r^2_{i-1/2}) \cdot (1 - p_i) \qquad (9)$$

The outer boundary (fuel internal radius) is recorded as of the given time point, so we will search for the new radius positions from the fuel outer boundary:

$$\tilde{r}_{i-1/2} = \sqrt{\tilde{r}^2_{i+1/2} - \frac{(r^2_{i+1/2} - r^2_{i-1/2}) \cdot (1 - p_i)}{1 - \tilde{p}_i}} \qquad (10)$$

Here, $r_{i-1/2}$, p_i is the value of the radius on the boundaries of the calculation cells and porosity at the calculation cell center in the fuel pellet initial state; and $\tilde{r}_{i-1/2}$, $\tilde{p}_i$ is the value of the radius and porosity at the given time point.

Equations (9) and (10) are valid only with $r > r_0$, where r_0 is the radius of the central hole formed due to the pore migration.

Test problem

To test the fuel porosity and inner radius calculation model used in the study, we shall consider a test problem based on data presented by the authors in Lackey et al. 1972.

Experimental porosity values were obtained for vibrocompacted (pebble) fuel element with high initial porosity of the $U_{0.85}Pu_{0.15}O_{2.0}$ fuel irradiated for 28 effective days: the linear power density was 44.62 W/mm, and the burnup was 0.7% of h.a. The initial porosity of non-irradiated fuel is $p_0 = 0.186$ rel. units, the external radius of fuel is $r_2 = 3.2$ mm, and the temperature on the outer surface is $T_2 = 550$ °C.

Fig. 2a (Lackey et al. 1972) shows the experimentally measured porosity values and the porosity distribution predicted by the pore displacement model (Lackey et al. 1972) and the dependence for describing the thermal conductivity of fuel.

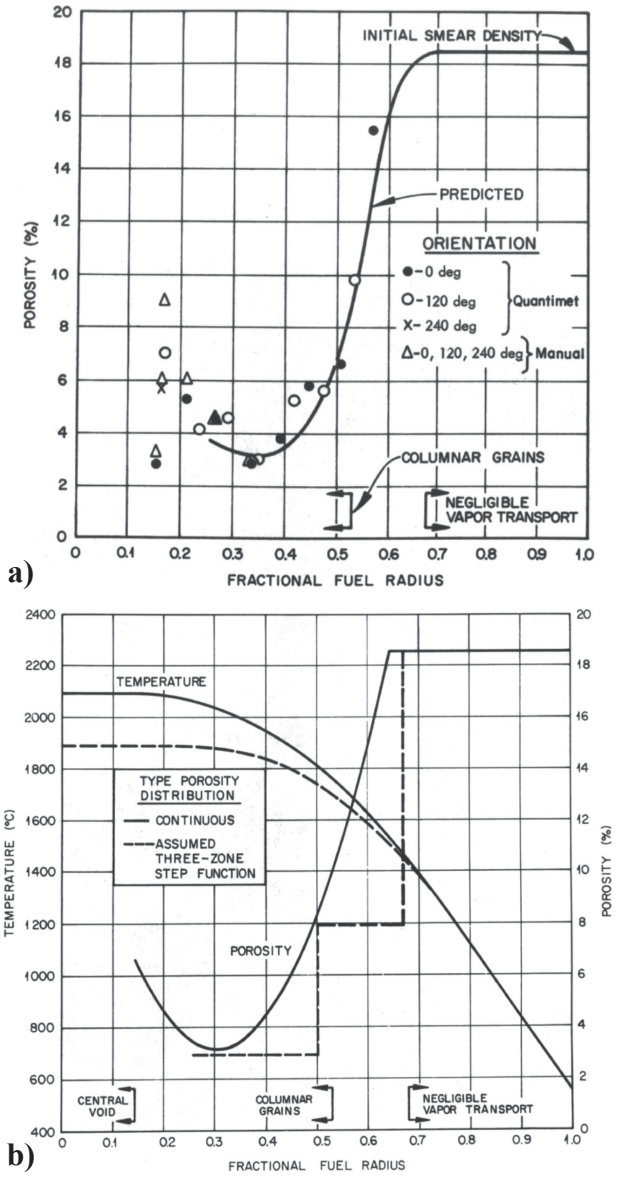

Figure 2. Position of the calculated curves for the porosity and temperature distribution along the fuel pellet radius, and experiment results (Lackey et al. 1972).

Fig. 2b (Lackey et al. 1972) shows the effect of the porosity distribution on fuel temperature. The results of the porosity calculation are presented in accordance with the assumption that fuel restructuring to 97% of the theoretical density takes place when a temperature of 1750 °C is exceeded, and to a density of 92% when the temperature is in a range of 1450 °C to 1750 °C, while it does not change at temperatures of below 1450 °C. The maximum design temperature was 1900 °C (dashed line).

The solid line in Fig. 2b shows the temperature distribution along the fuel radius when using the porosity distribution obtained from experiments (Fig. 2a – symbols, Fig. 2b – approximating porosity curve) to solve the thermal conductivity problem. The maximum temperature value for such calculation option is ≈2100 °C (the solid line in Fig. 2b).

Options of using dependences to calculate the mox fuel thermal conductivity

Let us consider two options for dependences that describe the thermal conductivity of MOX fuel. A dependence of the following type is presented in Philipponneau 1992:

$$\lambda = \left(\frac{1}{(1.32 \cdot (x + 0.00931)^{1/2} - 0.0911 + 0.38 \cdot (Bu/100) + 2.493 \cdot 10^{-4} \cdot T)} + 88.4 \cdot 10^{-12} \cdot T^3 \right) \cdot FM \quad (11)$$

where λ is the thermal conductivity coefficient, W/(m·K); *Bu* is the burnup, % h.a.; *T* is the temperature, K; *O/M* is the stoichiometry; *x* is the deviation from stoichiometry, (2 – *O/M*) if (2 –*O/M*) < 0, then *x* = 0; and *FM* = (1 – *por*)/(1 + 2 · *por*) is the coefficient of dependence on porosity.

With regard for the data obtained for fresh fuel (2001, 2013, 2017) and irradiated fuel (1993, 2017), dependence (12) has been proposed Magni et al. 2020:

$$\lambda = 1.755 + (\lambda_0 - 1.755) \cdot e^{-\frac{Bu}{128.75}} \quad (12)$$

$$\lambda_0 = \left(\frac{1}{0.01926 + 1.06 \cdot 10^{-6} \cdot x + 2.63 \cdot 10^{-8} \cdot Pu + (2.39 \cdot 10^{-4} + 1.37 \cdot 10^{-13} \cdot Pu) \cdot T} + \frac{5.27 \cdot 10^9}{T^2} \cdot e^{-\frac{17109.5}{T}} \right) \cdot FM \quad (13)$$

Here, λ is the thermal conductivity coefficient, W/(m·K); *Bu* is the burnup, (Mw·day/kg of h.a.); *Pu* is the fraction of Pu in the fuel composition, rel. units; *T* is the temperature, K; *x* is the deviation from stoichiometry, (2 – *O/M*) if (2 – *O/M*) < 0, then *x* = 0; *FM* = (1 – *por*)$^{2.5}$ is the coefficient of porosity; and *por* is the porosity, rel. units.

Fig. 3 shows the thermal conductivity values predicted by dependences (11) and (13), and experimental values (Philipponneau 1992) for fresh (non-irradiated) $U_{0.8}Pu_{0.2}O_{1.98}$ fuel (Fig. 3a) and $U_{0.8}Pu_{0.2}O_{1.93}$ fuel (Fig. 3b) with a density of 95% of the theoretical density. In formula (13), as can be seen, the dependence of thermal conductivity on stoichiometry and the Pu fraction is small. For stoichiometric $U_{0.8}Pu_{0.15}O_2$ fuel with an initial density of 95%, the thermal conductivity values predicted by two dependences are close Magni et al. 2020.

Results of calculations using two types of the pore displacement rate computation dependences

It is noted in Lackey et al. 1972 that two approaches can be used to estimate the pressure in pores: one of these is to assume that all pores are open, and the pressure in them is equal to the pressure beneath the cladding, and the other is that pores in areas with a porosity of less than 0.1 rel. units (0.07 rel. units assumed in Degaltsev et al. 1987 are closed, and the pressure in them depends on the temperature in the given area and the pressure in the pore when they are closed. It is noted that the results of the experiment calculations using different approaches differ slightly (Lackey et al. 1972).

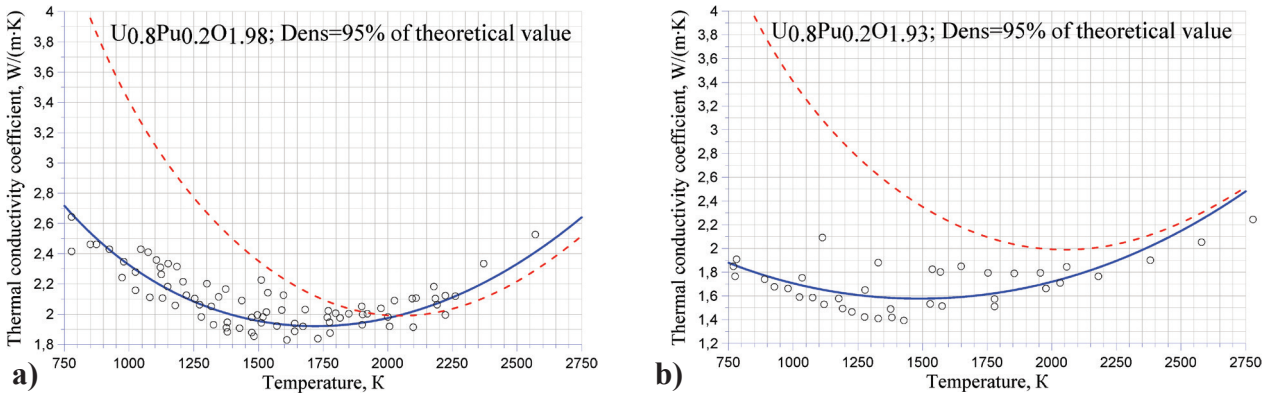

Figure 3. Thermal conductivity coefficient of MOX fuel as a function of temperature: solid blue line – dependence (11); dashed red line – dependence (13); circles show experimental data.

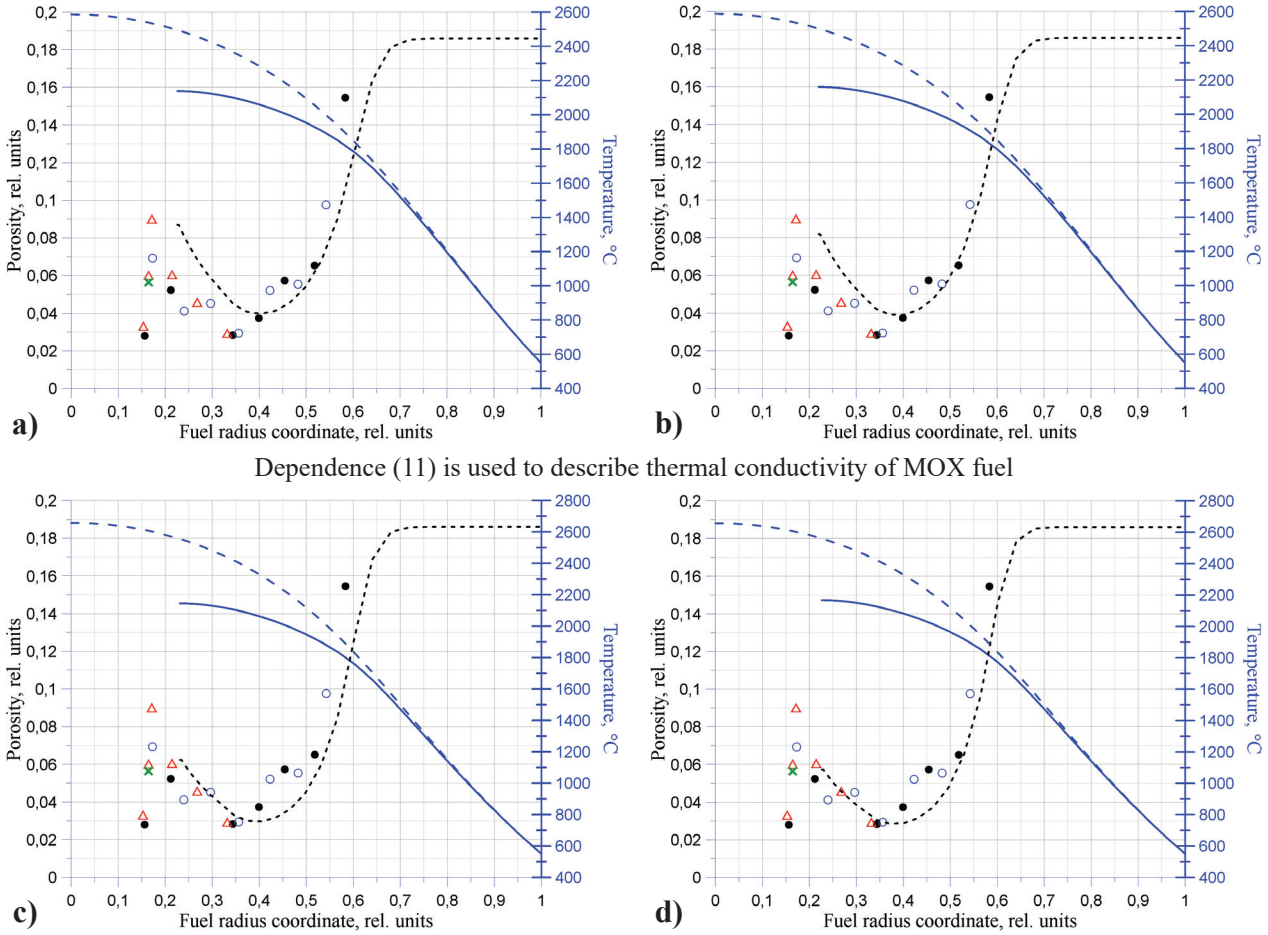

Figure 4. Positions of the calculated porosity and temperature distribution curves along the radius of the fuel pellet.

The paper presents the results of the test calculations using dependences (11) and (12) to describe the thermal conductivity of oxide fuel (the thermal conductivity equation is solved by double-sweep method). Fig. 4 presents the results of calculations performed assuming that all pores are closed, that is, the equations for the pore displacement rate include an expression for pressure (6). Positions are shown for the calculated curves of the porosity and temperature distribution along the fuel pellet radius with two pore displacement rate definition options used (the radius was initially broken down into 25 intervals). The dashed line shows the temperature distribution with the constant porosity of the pellet material, p_0 = 0.186 rel. units. Dependence (7) was used to define the pore displacement rate for Fig. 4a, c. Dependence (4) was used to deteremine the pore displacement rate for Fig. 4b, d (specified values: evaporation heat ΔH_{vap} = 600·10^3 J/mole; evaporation entropy ΔS_{vap} = 145 J/(mole·K)).

Fig. 5 shows calculations assuming that only some of the pores are closed (options: with porosity of less than 0.07 rel. units; with porosity of less than 0.1 rel. units); for open pores, pressure P_g used in the formulas will correspond to the pressure beneath the cladding. There is no initial and final pressure in the fuel rod shown in Lackey et al. 1972, so we assume that the pressure beneath the cladding is 1 atm (Fig. 5a, c), and 2.4 atm (Fig. 5b, d) (taking into account the fuel rod material temperature increase and thermal expansion). Dependence (4) is used to determine more accurately the pore displacement rate, and dependence (12) is used to describe the thermal conductivity of MOX fuel.

Conclusion

An algorithm consisting of a sequential solution to a thermal conductivity problem, taking into account the porosity in the calculation cell, determination of the pore displacement rate with calculating further porosity, and determination of new boundaries for the calculation cells allows one to obtain the time-dependent porosity and temperature distribution along the fuel radius.

Testing the algorithm based on an example of a real experiment has shown qualitatively consistent results in calculating the porosity distribution using an assumption that all pores are closed and assuming that there are regions with open and closed pores. At the same time, the maximum temperature in the fuel center, with restructuring taken into account, is close to the temperature calculated by the authors of Lackey et al. 1972 using experimental porosity distribution data.

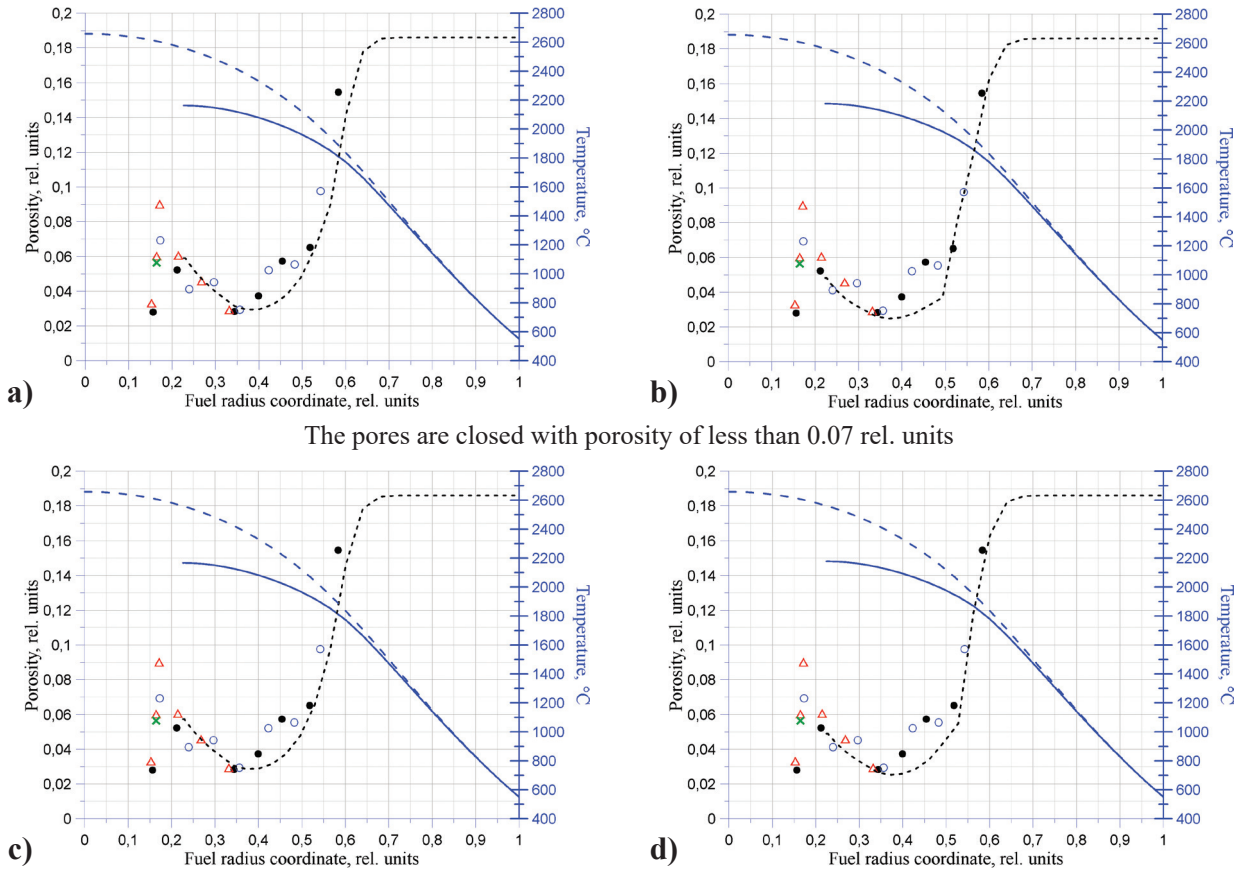

Figure 5. Positions of curves for the calculated porosity and temperature distribution along the fuel pellet radius assuming that there are open and closed pores.

References

- Bonev P, Chauvin N, Staicu D, Dahms E, Montagnier G, Papaioannou D, Dumas J-C, Boukhris I, Viallard I, Lainet M, Lamontagne J, Hanifi K (2023) New recommendation for the thermal conductivity of irradiated (U,Pu)O_2 fuels under fast reactor conditions. Comparison with recent experimental data. Journal of Nuclear Materials 577: 1–11. https://doi.org/10.1016/j.jnucmat.2023.154326
- Cappia F, Tanaka K, Kato M, McClellan K, Harp J (2023) Post-irradiation examinations of annular mixed oxide fuels with average burnup 4 and 5% FIMA. Journal of Nuclear Materials 533: 1–14. https://doi.org/10.1016/j.jnucmat.2020.152076
- Degaltsev YuG, Ponomarev-Stepnoy NN, Kuznetsov VF (1987) Behavior of high-temperature nuclear fuel under irradiation. Energoizdat Publ., Moscow, 208 pp. [in Russian]
- Freund D (1990) Fast reactor fuel structure evolution under irradiation. Kerntechnik 55(6): 350–357. https://doi.org/10.1515/kern-1990-550612
- Kinev EA (2011) The structure of pellet oxide fuel and its corrosive effect on the fuel pin cladding of the BN-600 reactor. Izvestiya vuzov. Yadernaya Energetika 1: 169–176. https://static.nuclear-power-engineering.ru/journals/2011/01.pdf [accessed Mar.15, 2024] [in Russian]
- Kozlov AV, Kinev EA, Tsygvintsev VA (2004) Post-reactor studies of oxide fuel after operation in the BN-600 reactor. VANT. Seriya: Materialovedeniye i novye materialy 2(63): 173–180. [in Russian]
- Lackey WJ, Homan FJ, Olsen AR (1972) Porosity and actinide redistribution during irradiation of (U, Pu)O_2. Nuclear Technology 16: 120–142. https://doi.org/10.13182/NT72-A31181
- Magni A, Barani T, Del Nevo A, Pizzocri D, Staicu D, Van Uffelen P, Luzzi L (2020) Modelling and assessment of thermal conductivity and melting behaviour of MOX fuel for fast reactor applications. Journal of Nuclear Materials 541: 1–13. https://doi.org/10.1016/j.jnucmat.2020.152410
- Olander DR (1976) Fundamental aspects of nuclear reactor fuel elements. Published by Technical Information Center, Office of Public Affairs Energy Research and Development Administration. The United States of America. https://doi.org/10.2172/7343826
- Parrish RJ, Cappia F, Aitkaliyeva A (2020) Comparison of radial effects of burnup on fast reactor MOX fuel microstructure and solid fission products. Journal of Nuclear Materials 531: 1–8. https://doi.org/10.1016/j.jnucmat.2020.152003
- Philipponneau Y (1992) Thermal conductivity of (U,Pu)O_{2-x} mixed oxide fuel. Journal Nuclear Materials 188: 194–197. https://doi.org/10.1016/0022-3115(92)90470-6
- Venkiteswaran CN, Jayaraj VV, Ojha BK, Anandaraj V, Padalakshmi M, Vinodkumar S, Karthik V, Vijaykumar Ran, Vijayaraghavan A, Divakar R, Johny T, Joseph Jojo, Thirunavakkarasu S, Saravanan T, Philip John, Rao BPC, Kasiviswanathan KV, Jayakumar T (2014) Irradiation performance of PFBR MOX fuel after 112GWD/t burn-up. Journal of Nuclear Materials 449: 31–38. https://doi.org/10.1016/j.jnucmat.2014.01.045